

# Investigation of Ablation Efficiency of Stainless Steel Using Pulsed Lasers in Burst Mode

Dirk Obergfell,\* Bahman Azarhoushang, and Andrés Fabián Lasagni

Due to its high corrosion resistance and mechanical properties, stainless steel is commonly used in various industrial applications. Although different types of stainless steel are similar in their chemical composition, they can differ significantly in their thermal diffusivity. This property is relevant in the ability of a material to conduct heat and thus, in laser processing. In this frame, this study compares the ablation efficiency and characteristics of polished stainless steel samples of the alloys AISI 304, AISI 420, and AISI 316Ti. They are irradiated with single ultrashort pulses having pulse durations between 250 fs and 10 ps as well as using GHz burst modii. The goal is to investigate the differences in both the ablation threshold and the ablation rate to improve the ablation efficiency.

The results show that shorter pulse durations lead to a more efficient ablation process. On the other hand, GHz bursts are found to be, in general, less efficient. In addition, there is a significant difference in the surface morphology depending on the process parameters. The differences in the thermal diffusivity do not significantly influence the ablation threshold fluence but surface morphology and the ablation rate.

requirements regarding their surface properties, these parts must be post-treated, which can be complex and energy intensive. Conventional methods, such as chemical etching, may not be environmentally friendly due to the use of toxic chemicals. However, ultrashort-pulsed laser processing presents a way to modify them in a digital way.<sup>[2]</sup> Furthermore, this process has several advantages over traditional manufacturing techniques, such as coating deposition, making it increasingly popular for various applications. Additionally, it does not generate waste in terms of chemicals or worn tools, making it an environmentally friendly technology.

Since in many sectors, such as the medical and food industry, the used parts are susceptible to temperature, it is relevant in laser processing to understand and control the impact on heat accumulation induced by laser radiation. For example, the treated parts must not have microcracks

to maintain high corrosion resistance. In this context, it has been shown that a relevant heat-affected zone is induced when utilizing pulse duration above 15 ps.<sup>[3]</sup> This means that only shorter pulses come into consideration for surface treatment.<sup>[4]</sup> On the other hand, the pulse duration can also significantly affect the ablation rate as well as the quality of the obtained surfaces.<sup>[5]</sup> In addition, comparative studies regarding the ablation behavior of different types of stainless steel have not been done so far.

Another parameter that can affect the ablation rate and surface quality is the implementation of bursts of pulses. With this mode, a single pulse is divided into a train of pulses, reaching repetition rates (temporal separation within the subpulses) in the GHz range. Previous studies have, for instance, shown that using 3–5 bursts can lead to high ablation rates of about  $2.5 \mu\text{m}^3 \mu\text{J}^{-1}$ . The main advantage of the burst is that it enables to work closer to the threshold fluence at the same scanning speed compared to a single pulse.<sup>[6]</sup> On the other hand, it was also reported that GHz bursts could lead to a reduction of the removal (ablation) rate for AISI304 steel by 90%.<sup>[7]</sup> Similar effects have been found for copper (75% reduction).<sup>[7]</sup> Shielding effects and melt redeposition are named as the main reason for this behavior.<sup>[8]</sup> In contrast, soda lime glass substrates could be treated with higher ablation rates. This effect was attributed to the non-linear absorption behavior exhibited by this material.<sup>[9]</sup> Additionally, burst-mode ablation has been associated with a decrease in energy efficiency for pulse delays from 300 ps to 20 ns, but advantages in terms of surface quality were reported.<sup>[10]</sup>


## 1. Introduction

Stainless steel is widely used in various industrial fields, including the medical and food industries.<sup>[1]</sup> In addition, the surface characteristics of products made of these alloys can affect different properties such as their corrosion resistance, heat transfer, biocompatibility, and bacteria adhesion. Thus, to meet specific

D. Obergfell, B. Azarhoushang  
Institute of Precision Machining (KSF)  
Furtwangen University  
Katharinenstrasse 2, 78532 Tuttlingen, Germany  
E-mail: dirk.obergfell@mailbox.tu-dresden.de

D. Obergfell  
Institute for Manufacturing Technology  
Technische Universität Dresden  
George-Bähr-Str. 3c, 01069 Dresden, Germany

A. F. Lasagni  
Fraunhofer-Institut für Werkstoff- und Strahltechnik IWS  
TU Dresden and Fraunhofer IWS  
Winterbergstr. 28, 01277 Dresden, Germany

 The ORCID identification number(s) for the author(s) of this article can be found under <https://doi.org/10.1002/adem.202300757>.

© 2023 The Authors. Advanced Engineering Materials published by Wiley-VCH GmbH. This is an open access article under the terms of the Creative Commons Attribution License, which permits use, distribution and reproduction in any medium, provided the original work is properly cited.

DOI: 10.1002/adem.202300757

Therefore, the effects of the above-mentioned parameters are relevant to be investigated in terms of ablation thresholds and rates depending on the steel type, allowing to determine how to process such materials with higher efficiencies compared to single pulses.

The goal of this work is to investigate the effect of the pulse duration and burst characteristics on the ablation threshold and rate for different stainless steel alloys, namely, AISI 304, AISI 420, and AISI 316Ti. These materials have been selected due to their dissimilar thermal diffusivities, which might lead to significant differences in their ablation behavior as well as their relevance in the medical sector. Single-pulse experiments are conducted to investigate the ablation mechanism of different types of stainless steels. Also, the impact of the ablation threshold on the surface morphology is studied. Finally, the ablated volume is calculated and compared with the total laser energy used.

## 2. Experimental Section

### 2.1. Materials

For the structuring experiments, 1 mm-thick stainless steel samples (HSM Stahl- und Metallhandel, Germany) of AISI 304 (X5CrNi18-10), AISI 420 (X46Cr13), and AISI 316Ti (X6CrNiMoTi1) with a size of  $\approx 30 \times 30$  mm were used. These alloys were of special interest due to their importance within the medical industry. Prior to the laser treatment, the samples were polished with a polishing machine (Metkon Forcipol 102, Germany) leading to a surface roughness  $R_a$  of  $0.1 \mu\text{m}$  and a flatness  $FLT_p$  lower than 20 nm. Following the polishing process, the samples were cleaned with ethanol. After the laser process, the samples were stored under atmospheric conditions and without any other additional treatment.

Due to the different thermal properties of the used materials, significantly different thermal diffusivities  $\alpha$  can be calculated using Equation (1)<sup>[11]</sup>

$$\alpha = \frac{k}{\rho c} \quad (1)$$

where  $k$  is the thermal conductivity,  $\rho$  the density, and  $c$  is the specific heat capacity. The obtained diffusivities together with the used material properties are listed in Table 1. It can be seen that the thermal diffusivity of the AISI 420 steel was significantly higher compared to both AISI 304 and AISI 316Ti steels.

**Table 1.** Material properties of the used stainless-steel alloys in this study (extracted from the manufacturer data sheets).

Material type	Thermal conductivity $k$ [W (m K) <sup>-1</sup> ]	Specific heat capacity $c$ [J (kg K) <sup>-1</sup> ]	Density $\rho$ [kg m <sup>-3</sup> ]	Thermal diffusivity $\alpha$ [m <sup>2</sup> s <sup>-1</sup> ]
AISI 420: X46Cr13	30	460	7700	$8.47 \times 10^{-6}$
AISI 304: X5CrNi18-10	15	500	7900	$3.80 \times 10^{-6}$
AISI 316Ti: X6CrNiMoTi1	15	500	8000	$3.75 \times 10^{-6}$

### 2.2. Laser Ablation Treatment

The laser treatments were carried out using a five-axis laser machine (GFMS LP400u, Switzerland). The system was equipped with a solid-state ultrashort-pulsed laser source (LightConversion Carbide CB-3, Lithuania), emitting a fundamental wavelength of 1030 nm. The laser source enabled to adjust the pulse duration in a range from 250 fs up to 10 ps. Furthermore, the burst-mode function could be applied, splitting the main pulse into 3–5 sub-pulses. The laser had a maximum average power of 40 W, with a maximal pulse energy  $E_p$  of 200  $\mu\text{J}$ . The laser beam was deflected on the surface using a galvanometer scanner (Scanlab Excelliscan, Germany) equipped with f-theta lens having a focal distance of 160 mm. This optical setup led to a beam diameter  $\omega_0$  of  $\approx 36 \mu\text{m}$ . The value of the applied laser fluence  $\phi$  can be calculated according to Equation (2).

$$\phi_{av} = \frac{E_p}{\pi\omega_0^2} \quad (2)$$

A range of laser parameters were tested, with pulse durations from 250 fs to 10 ps (see Table S1, Supporting Information) to investigate the ablation mechanism of the different types of stainless steel materials used in this work. The optical setup was kept the same in order to make all used parameters comparable. For each ablation experiment, five repetitions for each laser parameter were conducted and evaluated to obtain statistical certainty. For the burst parameters, picobursts (pb) were used. This means, that the intraburst pulse separation time was 450 ps, corresponding to a burst repetition frequency of 2.22 GHz. To investigate the influence of the pulse duration and the burst mode, the pulse duration was varied also from 250 fs to 10 ps, and burst of 3–5 pb was used.

Since single-ablation experiments were performed in this study, the produced craters are separated from each other and thus the motion accuracy of the system was not relevant.

### 2.3. Surface Characterization

An optical microscope (Keyence VHX-3000, Japan) was used to measure the diameters of the laser generated spots. For analyzing the ablated volume, a confocal microscope (Nanofocus  $\mu\text{Surf}$ , Germany) was utilized. Finally, scanning electron microscope (SEM) images were taken on selected samples (XL30 ESEM, Philips, Netherlands) for a better evaluation of the produced surface topology.

## 3. Results and Discussion

### 3.1. Determination of the Fluence Ablation Threshold

In a first set of experiments, the ablation threshold was investigated for the three used materials using the Liu method.<sup>[12]</sup> In this approach, the ablation threshold can be calculated out of the crater diameter that is produced from single-pulse experiments when the laser spot has a Gaussian spatial distribution.<sup>[13]</sup> This value is a good indicator on how much energy is needed for ablating the respective material and can be partially correlated to

optical abortion as well as heat diffusion.<sup>[14]</sup> Thus, these experiments attain to determine correlations between the ablation threshold with the thermal properties of the investigated materials as well as the pulse duration. Furthermore, the influence of GHz bursts is also investigated, with the aim of enhancing the ablation efficiency by distributing the laser pulse energy using the mentioned strategy.

**Figure 1** shows the squared diameter of the craters plotted over the average fluence used for the three investigated materials. The results corresponding to the three pulse durations are given (250 fs, 1 ps, and 10 ps). Additional results performed using other pulse durations are shown in the Supporting Information.

In **Figure 1a**, it can be observed for the AISI 420 stainless steel that the diameters of the produced craters for the different pulse durations are very similar within the lower-to-moderate fluence range (from  $\approx 1$  to  $8 \text{ J cm}^{-2}$ ). Only for higher-fluence levels significant differences are observed. Particularly, it can be seen that the craters produced with shorter pulse durations (250 fs and 1 ps) are larger compared to those generated with longer pulses (10 ps). This enhancement in the efficiency can be attributed to the reduced thermal losses resulting when applying shorter pulses, as previously reported.<sup>[14]</sup> In addition, an increase in the slope of the ablation curves is visible for laser fluences higher than  $7\text{--}8 \text{ J cm}^{-2}$ . This effect may be attributed to the notable decrease in reflectivity observed at higher fluence levels, as reported by other researchers.<sup>[13]</sup> Another possible explanation might be linked to the transition of the ablation mechanism, from optical to thermal ablation.<sup>[14]</sup> In case of the lower fluences, it is assumed that the influence of thermal conductivity on the ablation process is marginal, and the optical regime dominates. In contrast, in the high-fluence regime, the proportion of thermal ablation increases. Consequently, the enhanced coupling of laser energy with the material results in higher ablation, ultimately leading to larger ablated areas.

In case of the AISI 304 stainless steel, see **Figure 1b**, also a rise in the slope of the curve was observed at fluences higher than  $8\text{--}10 \text{ J cm}^{-2}$ . In addition, the reported crater's diameters are also similar for fluences up to  $\approx 8 \text{ J cm}^{-2}$  for all used pulse durations. Different from the steel AISI 420, in the higher-fluence range (from  $\approx 8 \text{ J cm}^{-2}$ ), no significant differences in the crater diameters were visible for all pulse durations.

In case of the AISI 316Ti stainless steel sample, also differences for the lower laser fluences were observed, as shown in **Figure 1c**. The crater diameters at the low- and moderate-fluence regions begin at the same fluence levels as for the other two

stainless steel materials. However, as the laser fluence increases, the rate of increase (slope) of the square crater's diameter becomes significantly higher. Especially for higher fluences, the square diameters of the craters are significantly larger (e.g.,  $\approx 6500 \mu\text{m}^2$  for AISI 316Ti at  $\approx 15 \text{ J cm}^{-2}$  and 250 fs, compared to 4500 and  $5550 \mu\text{m}^2$  for AISI 304 and AISI 420, respectively). Additionally, for the shorter pulse durations (250 fs and 1 ps), the highest ablation areas were observed (almost independent of the fluence region).

When comparing the thermal diffusivities of the steels AISI 316Ti and AISI 304 (see **Table 1**), the values are very similar ( $3.80 \times 10^{-6}$  and  $3.75 \times 10^{-6} \text{ m}^2 \text{ s}^{-1}$ , respectively), which means that heat diffusion effects cannot explain the observed differences. For instance, the heat-affected zone that can be calculated from the thermal diffusion length ( $L_{\text{th}}$ ) defined as two times the root square of the thermal diffusivity multiplied by the pulse duration.  $\tau$  ( $L_{\text{th}} = 2 (\alpha \tau)^{1/2}$ ) is estimated to be  $\approx 2$  and  $12 \text{ nm}$  for 250 fs and 10 ps pulse durations, respectively.<sup>[15]</sup> Therefore, a possible explanation can be related to differences in the optical penetration depth of the laser radiation at the used wavelength for the different materials. More precisely, the different chemical compositions of these alloys can lead to different absorption coefficients. For instance, the presence of the molybdenum and titanium components could potentially result in different absorption properties, as previously reported.<sup>[16]</sup> Furthermore the different crystallization phases (AISI 420 is a martensitic steel type, whereas AISI 304 and AISI 316Ti are austenitic steels) of the alloys could lead to absorption coefficient changes, which results in different absorption lengths.<sup>[17]</sup>

Out of the curves shown in **Figure 1**, the threshold fluences for the different steel types and used pulse durations can be extracted from the intersection of the fitting lines, for the low-fluence range, with the x-axis (laser fluence). The obtained values are plotted against the pulse duration in **Figure 2**. The results show that the threshold remains relatively constant (from  $0.30$  to  $0.50 \text{ J cm}^{-2}$ ) for the different pulse durations, with a slight tendency to decrease for the shortest used pulse duration of 250 fs ( $0.25\text{--}0.40 \text{ J cm}^{-2}$ ).

The lowest threshold values were reported for the AISI 420 stainless steel ( $\approx 0.1 \text{ J cm}^{-2}$  lower), which cannot be explained by heat diffusion effects, since this material presents the highest thermal diffusivity ( $8.47 \times 10^{-6} \text{ m}^2 \text{ s}^{-1}$ , see **Table 1**), as described before. Therefore, it is assumed that the same mechanisms described above (different chemical composition

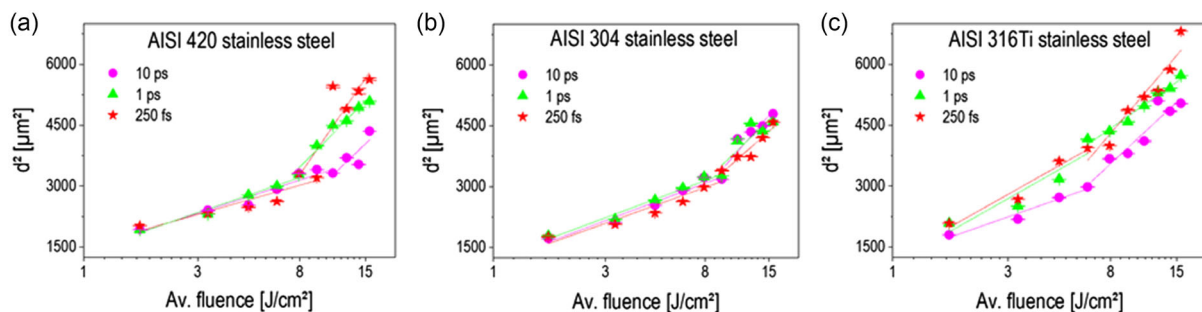


**Figure 1.** Squared crater's diameter depending on the used average fluence for a) AISI 304, b) AISI 420, and c) AISI 316Ti stainless steels.

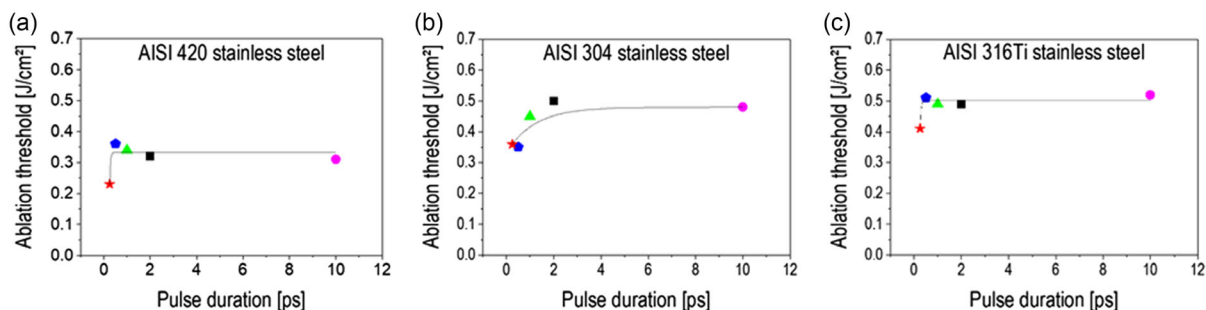


**Figure 2.** Calculated ablation thresholds depending on the used pulse duration for a) AISI 420, b) AISI 304, and c) AISI 316Ti. The lines are for the guidance of the eyes.

and different crystallization phases) can be responsible for the differences in ablation threshold.<sup>[16,17]</sup>

After determining the ablation thresholds for the single-pulse ablation experiments, the influence of the burst mode was investigated. **Figure 3** shows the obtained squared crater's diameter in AISI 304 material as a function of the used laser fluence for 250 fs and 10 ps pulses, using 3 and 5 picobursts (pb) (additional data for AISI 420 and AISI 316Ti steels is depicted in the Figure S2, Supporting Information). Compared to the results from the single-pulse ablation experiments shown in Figure 1b, the crater diameters are larger. This can be attributed to heat accumulation effects resulting from the very short interburst temporal separation.<sup>[18]</sup>

In addition, also, in this case, two distinct ablation regimes are visible for all pulse durations and the number of bursts (3 and 5 pb). The only appreciable difference is that this transition seems to occur at a lower fluence level (5–7  $\text{J cm}^{-2}$ ). Finally, remarkable differences were observed between the used longer and the shorter pulse durations (250 fs and 10 ps). Also, any significant difference was observed for 3 and 5 pb. Regarding the stainless steels AISI 420 and AISI 316Ti, similar results were observed (see Supporting Information).

### 3.2. Surface Morphology of the Produced Craters

An additional parameter that is relevant for determining possible differences between the used pulse durations and number of

picobursts (pb) is the surface topology of the produced craters. Consequently, SEM investigations were performed on selected samples.

For instance, SEM images of craters produced using 10 ps and 250 fs single pulses on all treated materials are presented in **Figure 4**. In all images, the circular shape of the produced craters is visible. In addition, additional features are visible that can be described as laser-induced periodic surface structures (LIPSS). These features have slight differences depending on the used pulse duration or within the modified region. Firstly, the produced LIPSS features in the external part of the craters show in general a circular shape that can be explained by the circular polarization of the laser beam.<sup>[19]</sup> This is visible, for instance, in Figure 4b,f. Furthermore, these circular-oriented microstructures are more distinct for the shorter pulse duration (250 fs), see Figure 4b,d,f for AISI 420, AISI 304, and AISI 316Ti materials, respectively. It has to be mentioned that LIPSS features generally occur after the application of several pulses, which explains, in this case, the observed irregularities in the structures.

On the other hand, in the central area of the craters where the laser intensity is higher, the produced structures exhibit an irregular morphology, with some resolidified material. This effect occurs for both 250 fs and 10 ps pulse durations. The transition of the observed topographies (from the center to the external areas) has already been reported by other authors and explained in terms of the local variation of the applied laser fluence.<sup>[20]</sup>

An additional effect that is observed in the case of the steel AISI 304 (Figure 4c,d) is the presence of line-like LIPSS that

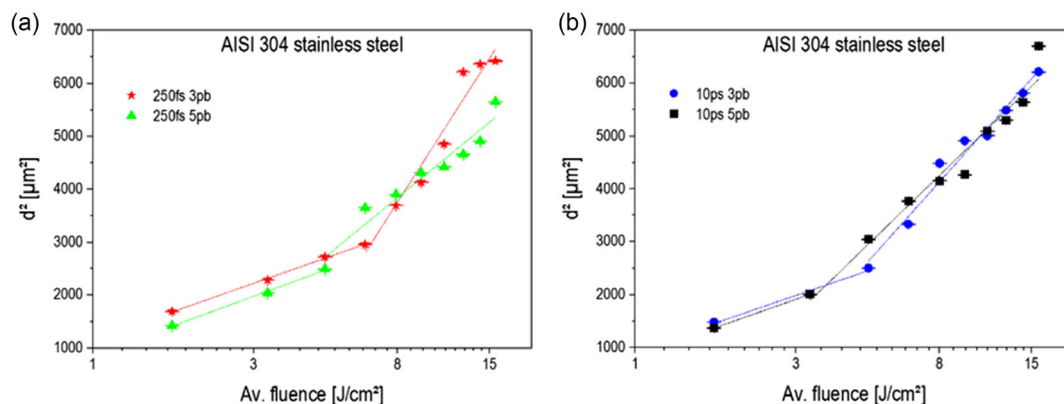


**Figure 3.** Squared crater's diameter of burst-mode ablation with a) 10 ps and b) 250 fs as well as 3 and 5 picoburst (pb). Material: AISI 304.

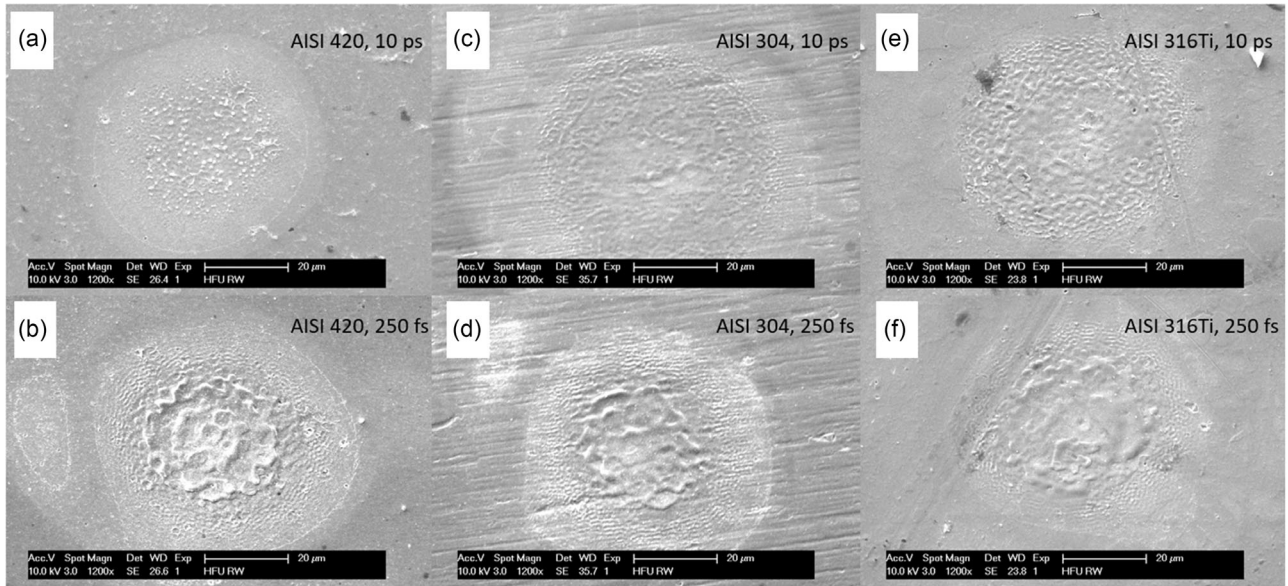


**Figure 4.** SEM images of single-pulse experiments performed with a,c,e) 10 ps and b,d,f) 250 fs pulse durations. The irradiated materials are (a,b) AISI 420, (c,d) AISI 304, and (e,f) AISI 316Ti. The fluence applied was  $15.6 \text{ J cm}^{-2}$ .

are oriented parallel to the initial topography of the untreated material (which differs from the other steels). This effect can be explained since it is known that the initial surface roughness of a metal can accelerate the formation of LIPSS, as reported by other researchers.<sup>[19]</sup>

The above described findings are also supported by confocal images of the same craters, as shown in **Figure 5**. For instance, the maximum depth of the craters produced with a pulse duration of 250 fs is significantly higher compared to the 10 ps pulses. In the case of the AISI 304 material irradiated with a fluence of

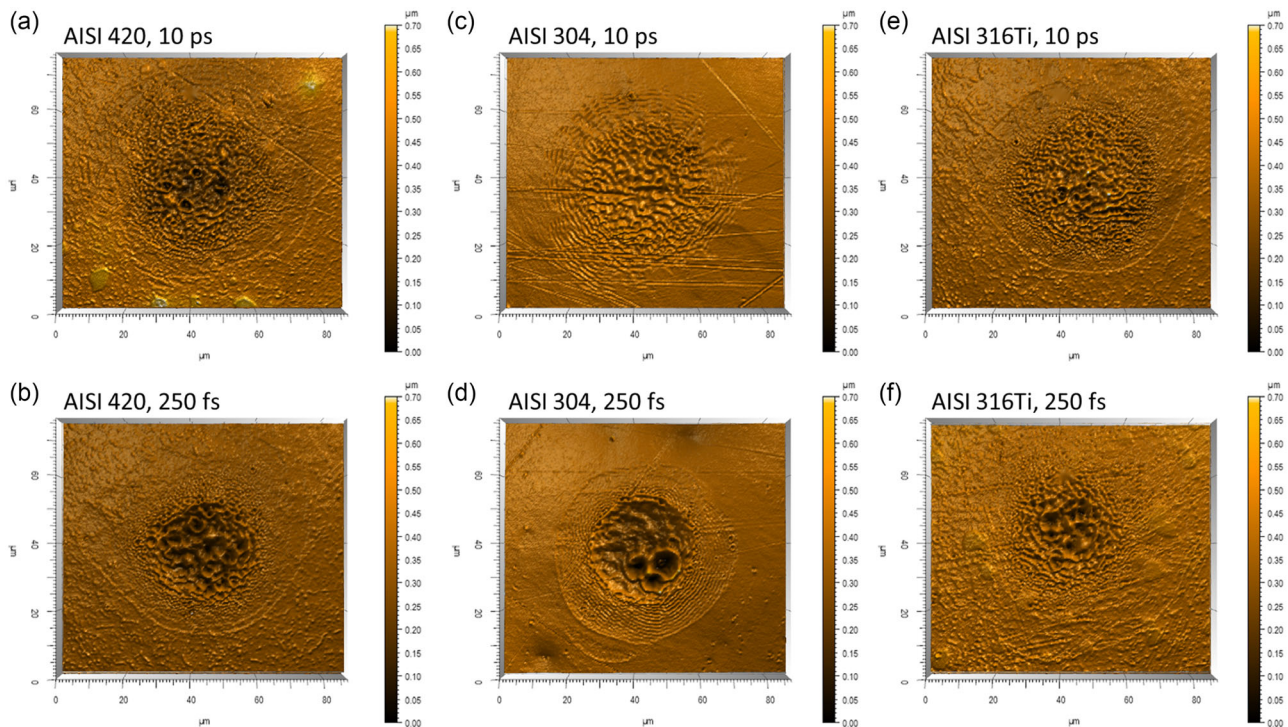


**Figure 5.** Confocal images of single-pulse experiments performed with a,c,e) 10 ps and b,d,f) 250 fs pulse durations. The irradiated materials are (a,b) AISI 420, (c,d) AISI 304 and (e,f) AISI 316Ti. The fluence applied was  $15.6 \text{ J cm}^{-2}$ .

$15.6 \text{ J cm}^{-2}$ , the maximal depth was  $\approx 0.5$  and  $\approx 0.3 \mu\text{m}$  for the 250 fs and 10 ps pulse durations, respectively.

Other information that can be obtained from the confocal images is related to the spatial period of the observed circular LIPSS. For the longest pulses (10 ps), the spatial period was larger compared to the shorter pulses (250 fs). For example, for the steel AISI 304, the measured periods are  $\approx 1.5$  and  $1.0 \mu\text{m}$  for 10 ps and 250 fs, respectively. Thus, in both cases, the circular produced LIPSS correspond to low-spatial-frequency LIPSS (LSFL) since they are close to the used laser wavelength.

Interestingly, the morphology of the produced craters using bursts of pulses is significantly different. This is shown in both **Figure 6** and **7**, corresponding to SEM and confocal images, respectively. These craters were also produced at the same fluence level as in the single-pulse images ( $\approx 15.6 \text{ J cm}^{-2}$ ) but using 3 and 5 pb.

When analyzing the morphology of produced craters in AISI 304 (**Figure 6**), with 250 fs and 10 ps pulse durations, a larger amount of resolidified material can be observed for all conditions (SEM images with the same laser parameters for AISI 420 and AISI 316Ti can be found in the Supporting Information). In addition, it can be seen that the main differences in the surface morphology arise from the number of bursts (3 or 5 pb) and not from the pulse duration. For example, the substrates irradiated with 3 pb (top images) with pulse durations of 250 fs (**Figure 6a**) and 10 ps (**Figure 6b**) only show additional rings in the central region compared to 5 pb. SEM images of the craters of AISI 420 and AISI 316Ti in burst mode are shown in **Figure S3** and **S4**, Supporting Information.

The effect of the smoother surface due to the larger amount of resolidified material can be explained due to the shorter inter-pulse distance (temporal) resulting from the burst mode (450 ps). In this case, after the first pulse of the burst hits and

melts the material surface, due to the shorter temporal distance between the burst pulses, the second (and subsequent pulses) arise to the surface before resolidification occurs. Thus, there is not sufficient time for heat conduction resulting in a larger amount of molten material.<sup>[21]</sup>

In addition, the observed rings in this case might not correspond to LIPSS features but are caused by interference effects. These circular structures (also called Newton rings) are created due to the interplay of the shockwave, ablation, and plasma dynamics. The shockwave generated by the laser pulse reflects and interacts with itself and the surrounding plasma. These interactions can lead to constructive or destructive interference patterns, resulting in concentric rings around the initial laser pulse impact point.<sup>[22]</sup>

Finally, the surface topology of craters produced only with 250 fs of pulse duration using 3 and 5 pb on AISI 420, AISI 304, and AISI 316Ti is shown in **Figure 7**. Also in this case, the central region of the craters has deeper features that can be explained by the Gaussian distribution of the laser spot intensity. Similar to the SEM images, distinct rings around the central crater can be observed and classified as Newton rings.<sup>[22]</sup> In addition, the depth of the crater slightly decreases with a higher number of bursts. For the irradiated AISI 420 steel with a fluence of  $15.6 \text{ J cm}^{-2}$ , the maximal depth was  $\approx 0.4$  and  $\approx 0.3 \mu\text{m}$  for 3 and 5 pb (**Figure 7a,b**), respectively. This phenomenon could be attributed to plasma shielding effects.<sup>[23]</sup> Confocal images with the same laser parameters on AISI 304 are shown in **Figure 7c,d** and on AISI 316Ti in **Figure 7e,f**. No significant differences could be observed.

### 3.3. Ablation Rate Investigations

To determine the optimal process conditions for achieving the highest removal rate, an assessment of the ablated volume in

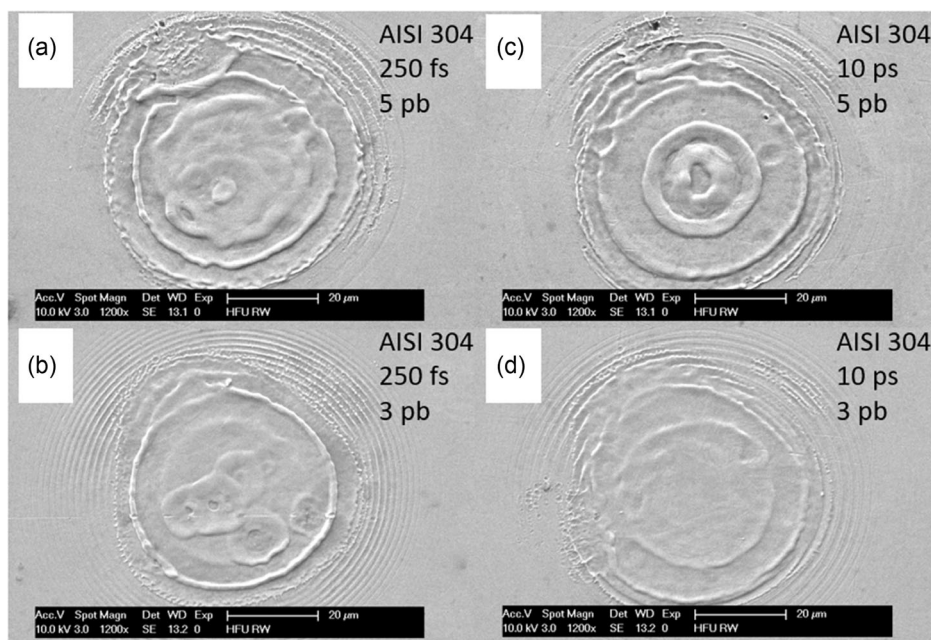


**Figure 6.** SEM images of AISI 304 substrate irradiated with burst mode with a,b) 250 fs and c,d) 10 ps. The images on the top (a,c) correspond to 5 pb, while on the bottom to 3 pb. The fluence applied to all samples was  $15.6 \text{ J cm}^{-2}$ .

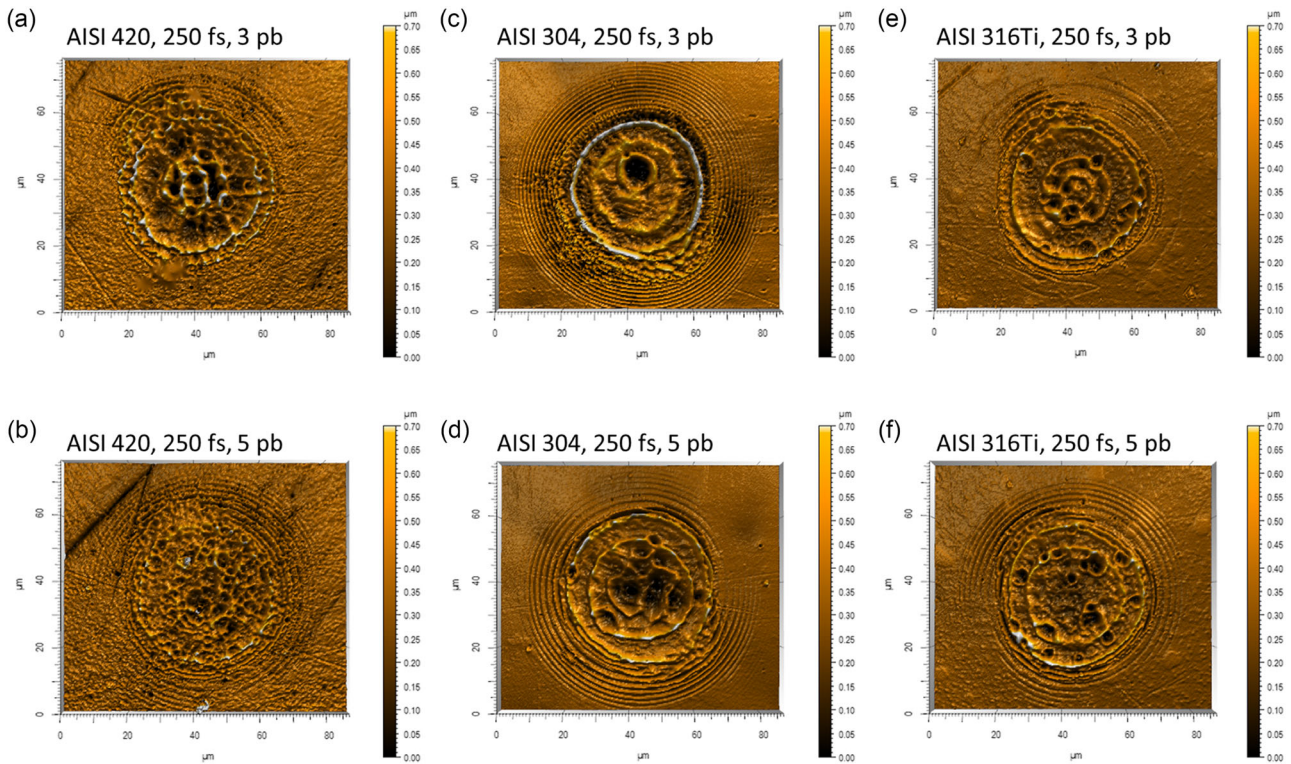


**Figure 7.** a–f) Confocal images of single pulses produced with a 250 fs pulse with 3 (top) and 5 pb (bottom). (a,b) AISI 420; (c,d) AISI 304, and (e,f) AISI 316Ti. The fluence applied to all samples was  $15.6 \text{ J cm}^{-2}$ .

relation to the applied energy per unit area (fluence) for each individual pulse was conducted. This involved calculating the ablated volume from the experiments presented in the previous sections.

The calculations are presented in **Figure 8** for all used materials when using single pulses at 250 fs and 10 ps, as well as 250 fs with 3 pb. It can be observed that for all three steel types, the shorter pulse duration results in a higher ablation volume at the same fluence levels. As in the curves showing the evolution of the squared crater diameter as a function of the laser fluence (Figure 1 and 3), the transition from the two different ablation regimes is visible. As mentioned before, while this change is evident in all materials, it does not occur at the same laser

fluence, consistent with similar observations made by other researchers.<sup>[23]</sup>

Furthermore, it is evident that craters generated using GHz burst mode exhibit a reduced amount of ablated material in all cases, consistent with previous research findings.<sup>[6]</sup> It has been described that an interpulse delay below 1 ns results in enhanced pulse interaction with the ablation plume.<sup>[24]</sup> Consequently, the ablation efficiency is reduced. Additionally, due to heat accumulation effects, more melt can be observed on the surface, as it has been mentioned in the previous sections. On the other hand, exploiting this phenomenon can be advantageous for achieving a smoother surface texture and, thus, interesting depending on the target application.<sup>[24]</sup>

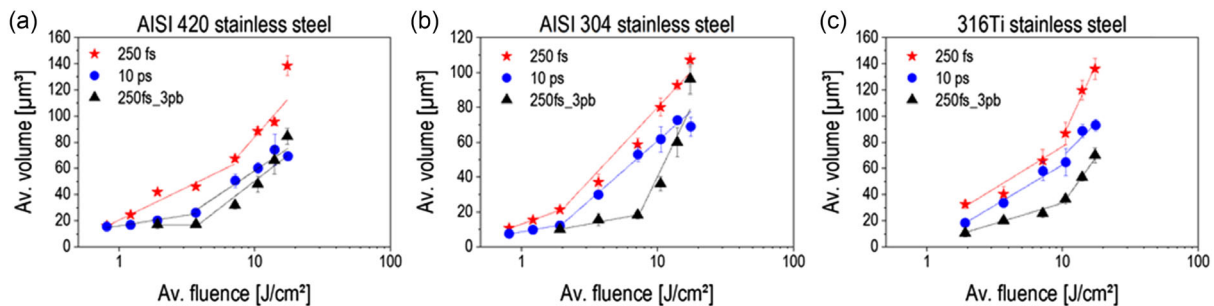


**Figure 8.** Ablated volume for single-pulse ablation experiments as a function of the applied laser fluence for a) AISI 420, b) AISI 304 and c) AISI 316Ti stainless steels.

Other effects that remain unclear are related to possible differences on the surface chemistry induced by the laser treatment on the utilized steels. In general, the treatment of steel surfaces (AISI 301, 304L, 316L) using fs and ps pulses is shown to oxidize the surface.<sup>[25–27]</sup> Due to the different concentrations in the allowing elements of the used steels, it could be possible also that different types of oxides (e.g., Cr<sub>2</sub>O<sub>3</sub>, Fe<sub>3</sub>O<sub>4</sub>) are predominantly formed on the surface.<sup>[28]</sup> These possible modifications have to be investigated in the future.

## 4. Conclusion

In this study, the ablation characteristics of three stainless steel types, namely, AISI 420, AISI 304, and AISI 316Ti, were investigated using single-ultrashort laser pulses and pulse burst modes. The focus was on examining the ablation threshold, surface morphology, and achievable ablation rates. Using a range of parameters between 250 fs and 10 ps, the results show any significant difference regarding the ablation threshold in the range between 1 and 10 ps ( $\approx 0.30\text{--}0.50\text{ J cm}^{-2}$ ). In case of the experiments conducted at shorter pulse durations (e.g., 250 fs), smaller ablation thresholds were calculated ( $\approx 0.25\text{--}0.40\text{ J cm}^{-2}$ ).

Regarding the surface morphology of the produced craters, significant differences were observed by comparing fs and ps pulses as well as when applying the burst mode. In the case of single-pulse laser ablation experiments (without bursts), the formation of LIPSS structures was observed, being more evident for the shorter pulse durations. In the case of the burst mode, the produced craters presented a significantly larger amount of molten materials, showing different ring features denoted as Newton rings and resulting from interference effects of the laser radiation with the produced plasma.

Finally, an analysis of the ablated volume indicated that shorter pulse durations resulted in higher material removal. In addition, the GHz pulse burst showed to be less efficient than the single pulses. Future investigations should explore the effects of repetition rate as well as irradiating larger areas to identify optimal parameters for energy-efficient material ablation.

## Supporting Information

Supporting Information is available from the Wiley Online Library or from the author.

## Acknowledgements

The research was partially funded by Hochschule Furtwangen. Open Access funding enabled and organized by Projekt DEAL.

## Conflict of Interest

The authors declare no conflict of interest.

## Data Availability Statement

The data that support the findings of this study are available from the corresponding author upon reasonable request.

## Keywords

ablation thresholds, laser–material interactions, stainless steels, ultrashort pulsed lasers

Received: May 21, 2023

Revised: July 10, 2023

Published online:

- [1] a) R. J. Narayan, in *Materials for Medical Devices*, ASM International, Russell Township, Geauga County, Ohio, pp. 199–210; b) D. A. K. Patel AD, *J. Mater. Sci. Eng.* **2015**, *4*, 5.
- [2] T. Graf, M. Hoßfeld, V. Onuseit, in *ARENA2036* (Eds: P. Weißgraeber, F. Heieck, C. Ackermann), Springer Berlin Heidelberg, Berlin, Heidelberg **2021**, pp. 386–393.
- [3] V. Zinnecker, S. Madden, C. Stokes-Griffin, P. Compston, A. V. Rode, L. Rapp, *Opt. Laser Technol.* **2022**, *148*, 107757.
- [4] D. Breitling, A. Ruf, F. Dausinger, *Proc. SPIE*, **49**, <https://doi.org/10.1117/12.541434>.
- [5] a) B. Lauer, B. Jäggi, B. Neuenschwander, *Phys. Proc.* **2014**, *56*, 963; b) B. Jaeggi, B. Neuenschwander, S. Remund, T. Kramer, *Laser Applications in Microelectronic and Optoelectronic Manufacturing (LAMOM) XXI*, SPIE LASE, San Francisco, CA **2017**, p. 100910; c) S. Remund, M. Chaja, Y. Zhang, B. Neuenschwander, *Laser Applications in Microelectronic and Optoelectronic Manufacturing (LAMOM) XXIV*, SPIE LASE, San Francisco, CA **2019**, p. 3.
- [6] a) T. Kramer, B. Neuenschwander, B. Jaeggi, S. Remund, U. Hunziker, J. Zürcher, *Phys. Proc.* **2016**, *83*, 123; b) B. Neuenschwander, B. Jaeggi, D. J. Förster, T. Kramer, S. Remund, *J. Laser Appl.* **2019**, *31*, 22203; c) J. Ströbel, B. Voisiat, K. Du, A. F. Lasagni, *Mater. Lett.* **2019**, *246*, 121; d) H. Le, T. Karkantonis, V. Nasrollahi, P. Penchev, S. Dimov, *Appl. Phys. A* **2022**, *128*, 711.
- [7] a) T. Hirsiger, M. Gafner, S. Remund, M. Chaja, A. Urniežius, S. Butkus, B. Neuenschwander, *Laser Applications in Microelectronic and Optoelectronic Manufacturing (LAMOM) XXV*, SPIE LASE, San Francisco, CA **2020**, p. 27; b) S. Butkus, V. Jukna, D. Paipulas, M. Barkauskas, V. Sirutkaitis, *MDPI Micromach.* **2020**, *11*, 733.
- [8] a) P. Lickschat, D. Metzner, S. Weißmantel, *J. Laser Appl.* **2021**, *33*, 22005; b) D. Förster, S. Faas, S. Gröninger, F. Bauer, A. Michalowski, R. Weber, T. Graf, *Appl. Surf. Sci.* **2018**, *440*, 926.
- [9] S. Remund, M. Gafner, M. Chaja, A. Urniežius, S. Butkus, B. Neuenschwander, *Proc. CIRP* **2020**, *94*, 850.
- [10] M. Sailer, F. Bauer, J. Kleiner, M. Kaiser, *LIM Proc.* **2015**, Corpus ID: 210916713.
- [11] R. J. Narayan, *Encyclopedia of Biomedical Engineering*, Elsevier Academic Press, Cambridge, MA **2018**.
- [12] J. M. Liu, *Opt. Lett.* **1982**, *7*, 196.
- [13] J. Winter, M. Spellauge, J. Hermann, C. Eulenkamp, H. P. Huber, M. Schmidt, *Opt. Express* **2021**, *29*, 14561.
- [14] D. J. Förster, B. Jäggi, A. Michalowski, B. Neuenschwander, *Materials* **2021**, *14*, 3331.
- [15] Y. Hirayama, Y. M. Obara, *J. Appl. Phys.* **2005**, *97*, 064903.
- [16] N. G. Henriksen, O. Z. Andersen, M. S. Jellesen, T. L. Christiansen, M. A. J. Somers, *HTM J. Heat Treat. Mater.* **2022**, *77*, 177.
- [17] B. Karlsson, C. G. Ribbing, *J. Appl. Phys.* **1982**, *53*, 9.
- [18] S. Gräf, *Adv. Opt. Technol.* **2020**, *9*, 11.
- [19] J. Bonse, S. Gräf, *Laser Photonics Rev.* **2020**, *14*, 2000215.
- [20] P. Lickschat, J. Schille, M. Müller, S. Weißmantel, G. Reißer, in *LIA Pub*, 615 = 105 (Ed: K. Washio), Laser Institute of America, Orlando, FL **2012**, pp. 1261–1268.
- [21] C. Gaudiuso, G. Giannuzzi, A. Volpe, P. M. Lugarà, I. Choquet, A. Ancona, *Opt. Express* **2018**, *26*, 3801.



- [22] J. Hernandez-Rueda, J. Siegel, M. Garcia-Lechuga, J. Solis, *J. Opt. Soc. Am. B* **2014**, *31*, 1676.
- [23] G. Giannuzzi, C. Gaudio, C. Di Franco, G. Scamarcio, P. M. Lugarà, A. Ancona, *Opt. Lasers Eng.* **2019**, *114*, 15.
- [24] M. Spellaugue, J. Winter, S. Rapp, C. McDonnell, F. Sotier, M. Schmidt, H. P. Huber, *Appl. Surf. Sci.* **2021**, *545*, 148930.
- [25] N. M. Bulgakova, M. Nadezhda, *Micromachines* **2014**, *5.4*, 1344.
- [26] C. Sciancalepore, L. Gemini, L. Romoli, F. Bondioli, *Surf. Coat. Technol.* **2018**, *352*, 370.
- [27] A. M. Kietzig, S. G. Hatzikiriakos, P. Englezos, *Langmuir* **2009**, *25*, 4821.
- [28] C. M. Abreu, M. J. Cristóbal, R. Losada, X. R. Nóvoa, G. Pena, M. C. Pérez, *Electrochim. Acta* **2006**, *51*, 2991.